ELSEVIER

Journal of Photochemistry and Photobiology
A: Chemistry 85 (1995) 11–21

Journal of
PHOTOCHEMISTRY
AND
PHOTOBIOLOGY
A:CHEMISTRY

Excited state relaxation channels of liquid-crystalline cyanobiphenyls and a ring-bridged model compound. Comparison of bulk and dilute solution properties

A.M. Klock[a], W. Rettig[a,*], J. Hofkens[b], M. van Damme[b], F.C. De Schryver[b,*]

[a]*Iwan-N.-Stranski-Institut, Technische Universität Berlin, Straße des 17. Juni 112, W-10623 Berlin 12, Germany*
[b]*Department of Chemistry, Katholieke Universiteit Leuven, Celestijnenlaan 200F, B-3001 Heverlee, Belgium*

Received 16 December 1993; accepted 5 May 1994

Abstract

The photophysical properties of 4-alkyl- and 4-alkoxy-4′-cyanobiphenyls with different chain lengths were compared in the dilute solution phase and bulk phases (crystalline, liquid-crystalline and isotropic) with respect to Stokes shifts and decay times. In solution, highly polar states are formed with decay times around 1 ns and subnanosecond rise times indicative of a molecular rearrangement occurring prior to emission. In the bulk phase, the major proportion of the emission derives from an excimer-type state with a red-shifted spectrum and very long decay time (10–25 ns depending on temperature and chain length). Possible excimer conformations are discussed. An excimer with a twisted geometry (twisted intramolecular charge transfer (TICT) excimer) is excluded by comparison with a bridged biphenyl system (fluorene derivative). The same compound also demonstrates that excited state intramolecular relaxation towards a 90° twist angle is unlikely. In polar solvents, relaxation occurs towards an increased planarity in accordance with the Rapp model. This conclusion is discussed in relation to results from quantum chemical calculations.

Keywords: Relaxation channels; Cyanobiphenyls; Ring-bridged model

1. Introduction

Alkyl- and alkoxycyanobiphenyls (*n*CBs and *n*COBs) with long chain lengths ($n \geqslant 5$) form liquid-crystalline phases, the photophysical properties of which have been reported [1–4]. It has been shown that long-lived excimers ($\tau = 5$–22 ns [1–3] depending on system and temperature) are formed, both in the mesophases and in the isotropic melt. In dilute solution, however, both groups of compounds exhibit only short fluorescence decay times (around 1 ns) [5], and possess (especially the alkoxy derivatives) very large Stokes shifts indicative of large excited state dipole moments [6]. The question arises as to whether, for monomeric species in solution or for luminescent excimers in the bulk phase, twisted conformations are populated in the excited state; for the *n*COBs, good donor (alkoxyphenyl) and good acceptor (benzonitrile) groups are linked by a flexible single bond and could, in principle, allow population of a twisted intramolecular charge transfer (TICT) state (for reviews, see Ref. [7]). TICT state formation may also be possible in the excimer (excited dimer) if one of the moieties is in the TICT state and is stabilized by the other moiety (self-solvated TICT state), as recently proposed to explain the long-lived, red- shifted fluorescence of aggregates of dimethylaminobenzonitrile derivatives [8].

We therefore undertook a comparative spectral and decay time study of various *n*CBs and *n*COBs, including a bridged derivative unable to form twisted conformations. Even if TICT state formation does not occur in the flexible donor–acceptor biphenyls, angular excited state relaxation (well known for biphenyls [9]) would still be expected, namely from the ground state conformation (twisted by about 30°) to the excited state equilibrium with a much smaller twist angle. A careful spectral and decay time analysis should enable us to determine the different relaxation possibilities for the biphenyls and the corresponding fluorene derivatives.

Finally, time-resolved spectra and global analysis are used to assess the possibility of the simultaneous existence of more than one excimer.

*Corresponding authors.

SSDI 1010-6030(94)03881-T

2. Experimental details

The biphenyls studied, together with their abbreviations, are given in Fig. 1.

The alkyl- and alkoxycyanobiphenyls were obtained from BDH (Knn and Mnn series) and used as received. 4COB was shown to be free from impurities by high performance liquid chromatography (HPLC).

2.1. Solution phase

The solvents used were of spectroscopic grade (Uvasol) and were obtained from Merck. All solution samples (concentration, approximately 10^{-5} M) were studied in 1 cm quartz cells and degassed by repeated freeze–pump–thaw cycles.

The absorption spectra were recorded on an SLM Aminco DW 2000 UV spectrophotometer. Corrected fluorescence spectra were taken on a SPEX Fluorolog with excitation near the maximum of the long- wavelength absorption band. The fluorescence spectra were taken under thermostatically controlled conditions (using the Mettler FP82 hot stage).

Time-resolved measurements were obtained using single-photon- counting equipment with a synchronously pumped, cavity-dumped dye laser as excitation source [10].

A global iterative reweighted reconvolution program on the non-linear, least-squares algorithm of Marquardt [11] was used to estimate the unknown parameters α_j and τ_j (in Eq. (1)). The entire decay profiles, including the rising edge, were analysed. Fluorescence decay curves at different wavelengths and time increments were analysed simultaneously according to Eq. (1), and the sample and reference decay time parameters (fluorescence response function of the detection system, about 80 ps full width at half maximum (FWHM)) were linked. The advantages of the global analysis method are the improved model testing capability and the accuracy of the recovered parameters in comparison with single curve analysis [12].

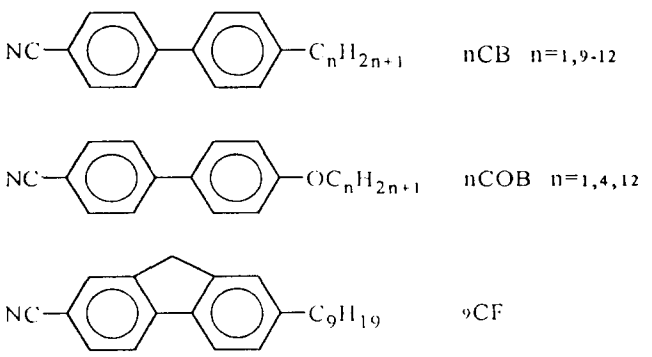

Fig. 1. Compounds investigated.

$$
\begin{aligned}
f_1 &= \sum_j \alpha_{j,1} \exp(-t/|\tau_j|) \\
f_2 &= \sum_j \alpha_{j,2} \exp(-t/|\tau_j|) \\
f_3 &= \sum_j \alpha_{j,3} \exp(-t/|\tau_j|) \\
&\vdots \\
f_i &= \sum_j \alpha_{j,i} \exp(-t/|\tau_k|)
\end{aligned}
\qquad (1)
$$

2.2. Bulk phase

The decay times and time-resolved spectra of neat phases were measured at the Berlin synchrotron radiation facility (BESSY) in the single-bunch mode (4.8 MHz, FWHM ≈ 500 ps) using single- photon-counting equipment [13]. The samples were measured through quartz plates with a layer thickness of about 20 mm in a thermostatically controlled, diagonally oriented cell holder. Time-resolved spectra were taken by setting an appropriate time window on the time-to-amplitude converter and recording the spectrum on a multichannel analyser in the multichannel scaling mode.

Steady state, corrected fluorescence spectra were taken on a Perkin–Elmer 650-60 fluorometer.

Quantum chemical calculations were carried out on a Convex C230 using the CNDO/S method [14]; 50 singly excited configurations were used for configuration interaction (CI) [15]. In additional calculations, 45 doubly excited states were found not to mix significantly with the singly excited states, with the lowest doubly excited state about 3 eV above the first singly excited state.

3. Results and discussion

Fig. 2 shows a comparison of the absorption and fluorescence spectra of 9COB in dilute solution and in crystalline, smectic and isotropic bulk phases. In solution, the spectra shift strongly to the red with increasing solvent polarity, but, in bulk phases, the spectral position corresponds in all cases to that of the strongly polar solvent. A small red shift is observed from the crystalline to the smectic phase, and a blue shift on further heating to the isotropic melt. The *n*CBs behave similarly. The intensity changes monitored at the blue or red edge of the spectra can be used to analyse the phase transitions, as shown previously [2–4]. Table 1 contains typical decay times measured in this work for bulk and solution phases and a comparison with literature data. In solution, all values are close to 1 ns. In bulk phases, long decay times of 10–25 ns prevail.

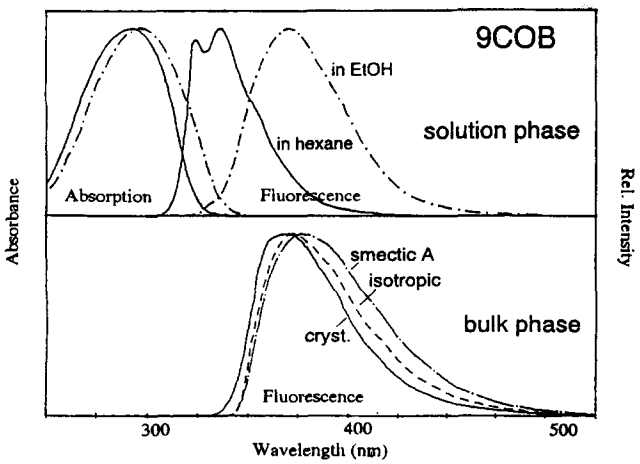

Fig. 2. Comparison of the absorption and fluorescence spectra of 9COB in dilute solution and the emission spectra in neat phases.

Table 1
Main fluorescence decay times of different alkyl- and alkoxycyanobiphenyls in neat phases (S, smectic A; N, nematic; I, isotropic, temperature dependent) and dilute solution at room temperature (if not stated otherwise, solutions are air saturated)

Compound	Environment (T (°C))	τ (main component) (ns)
1CB	Ethanol	1.15
7CB[a]	N(35)	19.4
	I(45)	14.1
8CB[a]	N(36)	19.2
	I(46)	15.1
9CB	N(48)	12.0
	I(54)	10.0
	Hexane	1.23
	Ethanol	1.14
10CB	N(46)	17.6
	I(54)	13.7
11CB	N(54)	11.6
	I(60)	8.0
12CB	N(50)	19.2
	I(63)	8.2
1COB	Ethanol	1.50
4COB[b]	Hexane	1.07
	Methanol	1.56
5COB	N(79)	8.5
	I(83)	7.5
	Hexane	0.92
	Ethanol	1.46

[a]Taken from Ref. [2], degassed solutions.
[b]Taken from Ref. [5].

To assess whether the large solvent-induced red shifts in solution and the strongly red-shifted excimer spectra are due to intramolecular twisting (TICT state formation), the remainder of this paper concentrates on a pair of bridged/unbridged biphenyls, namely on the spectral and fluorescence decay differences between 9CB and its planar fluorene derivative 9CF.

In section 3.1, the solution phase properties are discussed, and it is shown that molecular rigidity suppresses the typical behaviour of biphenyl derivatives, i.e. the blurring of the spectra at very low temperatures, and the occurrence of fluorescence rise times, both linked to the twisting relaxation of the phenyl rings towards planarity.

Section 3.2 deals with the excited state dipole moments and compares the results with quantum chemical calculations.

In section 3.3, the bulk phase properties of 9CB and 9CF are more closely examined, and time-resolved spectra and global analysis of fluorescence decays are used to extract the decay- associated spectra of 9CF. The two red-shifted components possess a rise time equal to the decay time of the short-wavelength component, establishing a mother–daughter relationship.

3.1. Twisting relaxation of biphenyls

Fig. 3 shows the absorption and emission spectra of 9CB and 9CF in an alkane solvent at room temperature. The absorption spectrum of 9CB is completely structureless and blue-shifted with respect to that of 9CF. The fluorescence spectrum shows considerable structure, although less than 9CF, sharing a more planar average conformation of 9CF in the ground state. For 9CF, the usual mirror image between the fluorescence and absorption spectra is observed, whereas for 9CB the different spectral shapes point to a major geometrical

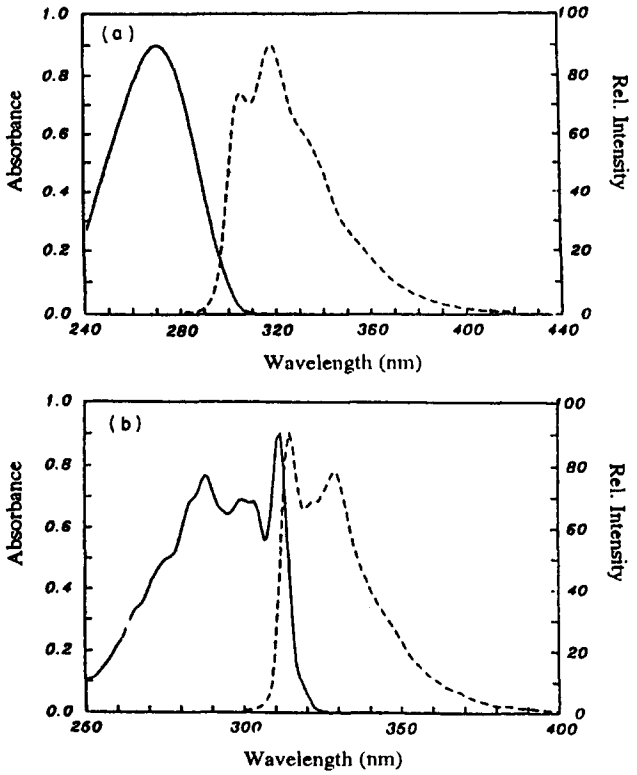

Fig. 3. Absorption and emission spectra of 9CB (a) and 9CF (b) in dilute n-hexane solutions.

rearrangement in the excited state. The more structured fluorescence of 9CB in comparison with the absorption band indicates a stiffening of the molecule in the excited state. The 0–0 emission of 9CF is situated at 315 nm, while that of 9CB is located at 305 nm, indicating a residual non-planarity in the relaxed excited state of 9CB.

Recently, a potential model has been put forward by Rapp and coworkers [9], accounting for the observed loss of vibrational structure of 9CB, and predicting an increase in the structure of the fluorescence band on cooling, and a loss of structure again below a certain temperature. This model is reproduced in Fig. 4. Due to the ground state steric hindrance to planarity, biphenyls are excited into twisted Franck–Condon (FC) conformations ($\Phi \neq 0°$) of the S_1 state. However, this state possesses a minimum for the planar conformation ($\Phi = 0°$). For viscosities which are not too high, the intramolecular twisting relaxation towards planarity is rapid such that thermal equilibrium is obtained in the S_1 state. For lower temperatures, the intramolecular rotational distribution function of the equilibrated S_1 state will narrow around $\Phi = 0°$, and therefore the spectra become more structured (energy spread $\Delta\epsilon_r$, see Fig. 4). If the temperature is lowered further, such that the relaxation from the FC conformation towards planarity is hindered or stopped, conformations with intermediate twist angles will also be able to emit, and the spectra will lose structure again (limiting energy spread $\Delta\epsilon_r$).

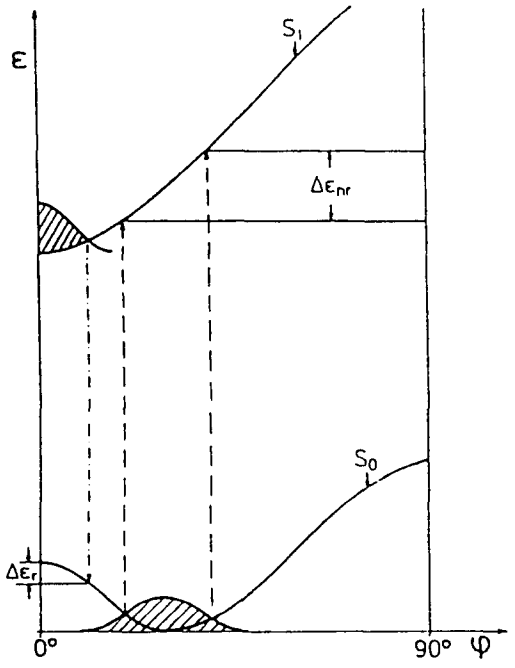

Fig. 4. Twist-angle-dependent potential energy scheme for biphenyl and related compounds (according to Ref. [9]). For explanation of $\Delta\epsilon$, see text.

This behaviour is also exhibited by the cyanobiphenyls studied here. Fig. 5 shows the spectra of 9CB at three different temperatures. A considerable gain in structure is observed on cooling to 183 K, but the structure is lost again by further cooling to 77 K. The spectra for 4COB are nearly identical. This figure also shows that the corresponding rigid compound 9CF does not exhibit this behaviour. Increasing structure is observed down to 77 K.

In their original paper, Rapp and coworkers [9] quantified the spectral structure by a structure factor S_R, which becomes small when the structure of the spectrum is high and tends towards unity for a complete loss of structure, i.e. when vibronic bands are not separated by an intensity minimum. Here, we use a structure factor S which is defined as

$$S = 1 - S_R = 1 - \frac{2I_v}{I_{p1} + I_{p2}} \quad (2)$$

In this way, S is largest when there is most structure. I_{p1} and I_{p2} are the intensities of the first and second vibrational peaks and I_v is the intensity of the valley in between. Fig. 6 displays the dependence of S on temperature for 9CF, 9CB and 4COB, which exhibits a behaviour very similar to 9CB. To obtain comparable data, corresponding peaks were chosen for P_1 and P_2. Thus, for 9CF, P_2 was assigned to the third peak, distant from P_1 by about 1400 cm^{-1} and corresponding to P_2 of 9CB (compare Fig. 5, peak separation about 1300 cm^{-1}). The minimum I_v close to P_1 was chosen for

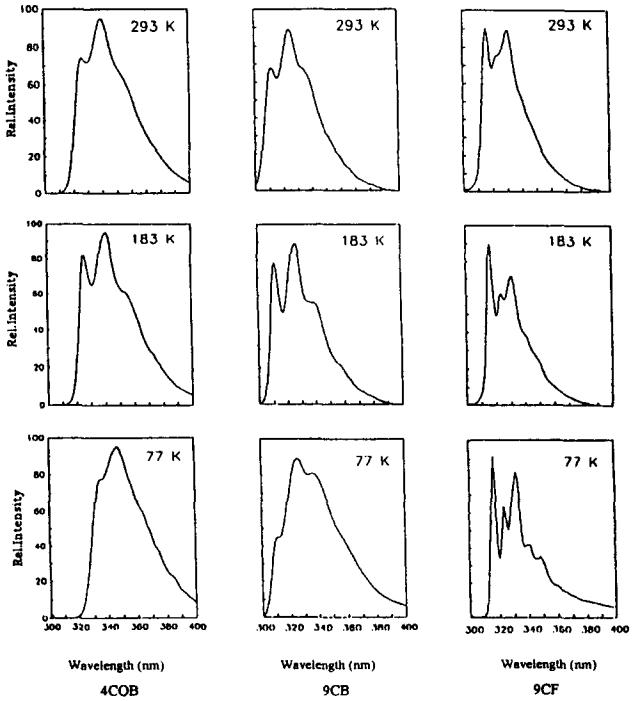

Fig. 5. Emission spectra of 9CF, 9CB and 4COB in *n*-hexane at different temperatures.

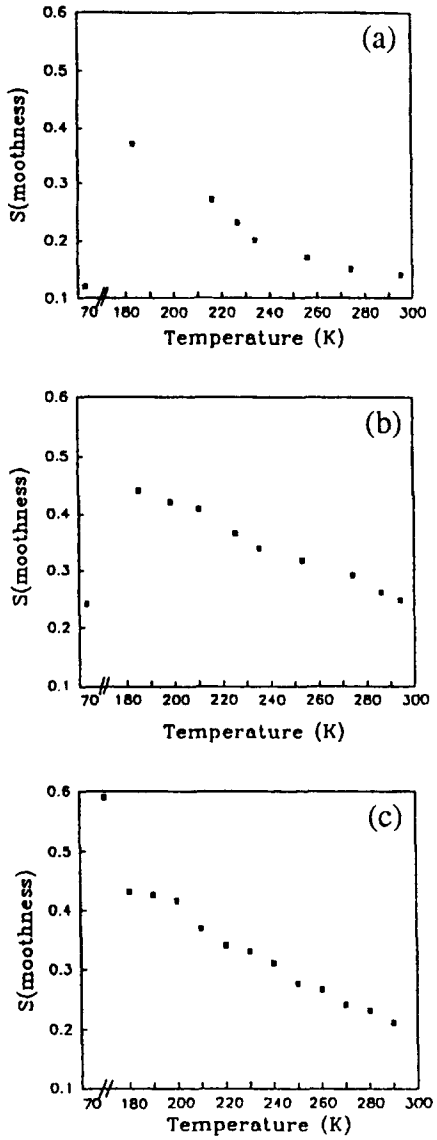

Fig. 6. Structure factors (S) as a function of temperature derived from the emission spectra of (a) 4COB/hexane; (b) 9CB/hexane; (c) 9CF/hexane.

9CF. As can be seen, the increased structure on cooling is reflected in higher S values for the three compounds, going from room temperature to 183 K. At 77 K, S becomes smaller again for 9CB and 4COB but even larger for 9CF.

The relaxation towards planarity for the cyanobiphenyls should also be visible in time-resolved experiments at room temperature and below, for sufficient time resolution of the detection equipment. The time resolution and precision can be increased by analysing several decay curves, taken under slightly different conditions, as channel time widths or emission wavelengths simultaneously by the global analysis method [12]. This approach has been used previously for 4COB [5], where rise time components were detected. In Table 2 the results obtained for 9CB and 9CF are compared.

Table 2
Rise and decay times of 9CB and 9CF in dilute solutions of different solvents at room temperature

Solvent	9CB		9CF	
	τ_{rise}	τ_{decay}	τ_{rise}	τ_{decay}
Isooctane	0.075	1.46	–	1.98
Diethylether	0.055	1.13	–	1.59
Ethylacetate	0.109	1.10	–	1.50
1-Butanol	0.261	1.08	0.241	1.30

In fast relaxing solvents (isooctane, diethylether and ethylacetate), 9CF shows purely monoexponential behaviour, whereas rise times between 55 and 110 ps are detected for 9CB which can therefore be ascribed to intramolecular rotational relaxation towards planarity. In the slowly relaxing solvent butanol, both compounds possess rise times of about 250 ps. In this case, therefore, the rise time is due to solvent relaxation. A similar solvent influence has been noted previously for TICT state formation kinetics [16]. In fast relaxing solvents, TICT state formation is controlled by the solvent viscosity alone, because for every intermediate twist angle the solvent is in equilibrium. However, in alcohol's, where the solvent relaxation times are considerably slower for a given viscosity, the relaxation towards the equilibrium condition is better described using two dimensions, twisting and solvent relaxation. Two-dimensional kinetic models of this kind have been developed recently [17].

3.2. Excited state dipole moment and electronic structure

With an increase in solvent polarity, the spectra of both 9CB and 9CF shift to the red and lose structure (Fig. 7). The spectra are analysed in Table 3. The red shift is due to the increased excited state dipole moment (μ_e) with respect to that of the ground state (μ_g) and can be evaluated using the Lippert equation [18]

$$\tilde{\nu}_{abs} - \tilde{\nu}_f = \frac{2(\mu_e - \mu_g)^2}{4\pi\epsilon_0 hca^3} \Delta f$$

$$\Delta f = \frac{\epsilon - 1}{2\epsilon + 1} - \frac{n^2 - 1}{2n^2 + 1} \quad (3)$$

where ϵ is the dielectric constant, n is the refractive index of the solvent and a is the radius of the Onsager cavity. A plot of $\tilde{\nu}_{abs} - \tilde{\nu}_f$ vs. Δf is shown in Fig. 8. As can be seen, the solvatochromic slope is very similar for the two compounds, and we therefore conclude that the dipole moment differences $\mu_e - \mu_g$ are similar.

Table 4 lists the solvatochromic slopes determined for different compounds. To convert these slopes into $\mu_e - \mu_g$ values, the Onsager radius a must be known.

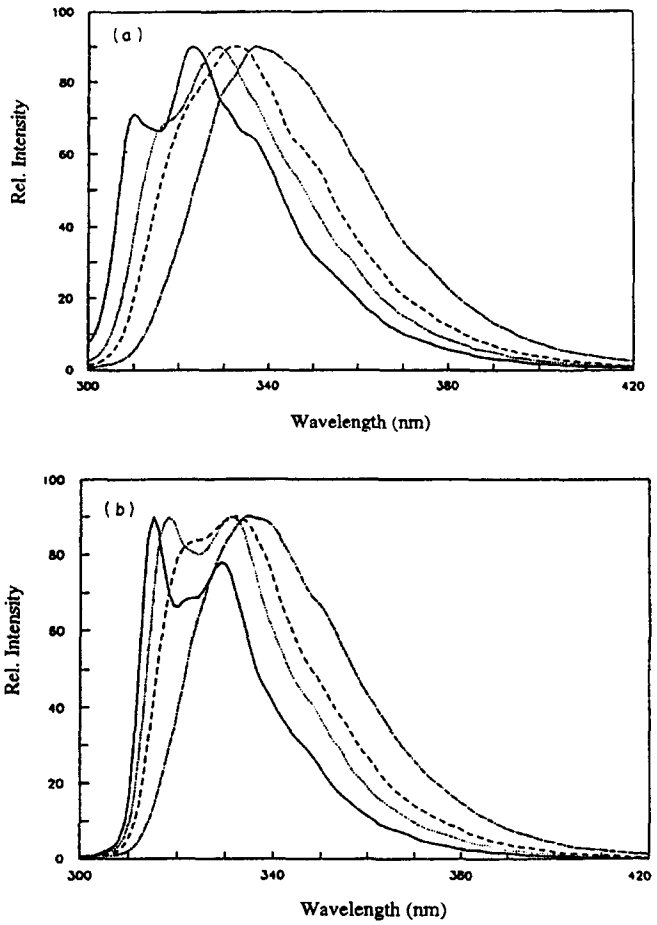

Fig. 7. Normalized fluorescence spectra of 9CB (a) and 9CF (b) in solvents of different polarity at room temperature: —, *n*-hexane; ···, diethylether; –, ethylacetate; -·-, acetonitrile.

For these highly elongated molecules, we chose to adopt a suggestion of Lippert [19] to take a as 40% of the long axis of the molecule; we base the determination of a on the elongated conformation of the molecules including the van der Waals' radii.

Table 4 contains two evaluations, one based on the shape of the whole molecule in the elongated conformation, including the long alkyl chain, and the other based on the size of the aromatic nuclei. Only the latter evaluation yields dipole moment values qualitatively consistent with the quantum chemical calculations in Table 5 (see below): $\mu(S_1)$ increases from *n*CB to *n*COB by 2–3 D. Comparison of Tables 4 and 5 and the short lifetimes measured in solution indicate that the emissive state of both *n*CBs and *n*COBs must be the ^1L_a-type state (S_3 for *n*CBs, S_2 for *n*COBs in the gas phase, according to the calculations) which is lowered in energy by solvent polarity. The assumption of $a = 40\%$ of the long axis of the aromatic core yields values for $\mu_{1,\,exp}$ (10–21 D) relative to $\mu_{1,\,calc}$ (10–12 D) which are too large. Further reduction of a to 30% would reduce this discrepancy ($\mu_{1,\,exp} = 13$–15 D).

The solvatochromic results indicate the following: (1) the ordinary Onsager–Lippert equation (Eq. (3)) has to be treated with caution for elongated molecules especially regarding the choice of a; (2) the alkyl chain, which does not belong to the aromatic system, should not be included in the determination of a; this is further substantiated by the similarity between the fluorescence spectra of *n*CBs and *n*COBs of different chain length ($n = 1$–12) [6,20].

The *n*COBs possess considerably larger excited state dipole moments than the *n*CBs, but 9CB and 9CF do not differ significantly; we therefore conclude that the emitting conformations are probably similar and that TICT state formation in 9CB is not supported by our results.

Further insight can be gained by quantum chemical calculations [21], the results of which are collected in Tables 5 and 6. The following observations can be made.

(1) As the strength of the donor group is gradually increased from *n*CB to dimethylaminocyanobiphenyl (DMA-CB), the nature of the S_1 state of the planar conformation changes from forbidden ($f < 0.01$, ^1L_b-type, transition moment M perpendicular to the long molecular axis z) to allowed ($f > 0$, ^1L_a-type, M parallel to z). The methoxycyanobiphenyl (1COB) and aminocyanobiphenyl (A-CB) compounds are borderline cases in which these two types of state are nearly degenerate. Due to

Table 3
Absorption and emission maxima (nm) of dilute solutions of 9CB and 9CF and emission halfwidths (cm^{-1})

Solvent	9CB			9CF		
	$\lambda_{max,A}$	$\lambda_{max,f}$	FWHM	$\lambda_{max,A}$	$\lambda_{max,f}$	FWHM
Isooctane	274.2	309	3670	287.6	315	2770
Dibutylether	275.7	315	3670	288.1	317	3080
Diethylether	278.2	329	3700	288.0	318	3220
Ethylacetate	279.2	332	3700	288.2	323	3350
1-Butanol	281.4	336	3700	289.8	336	3520
Acetonitrile	279.8	336	3680	288.4	336	3580
Methanol	280.0	338	3740	288.8	338	3640

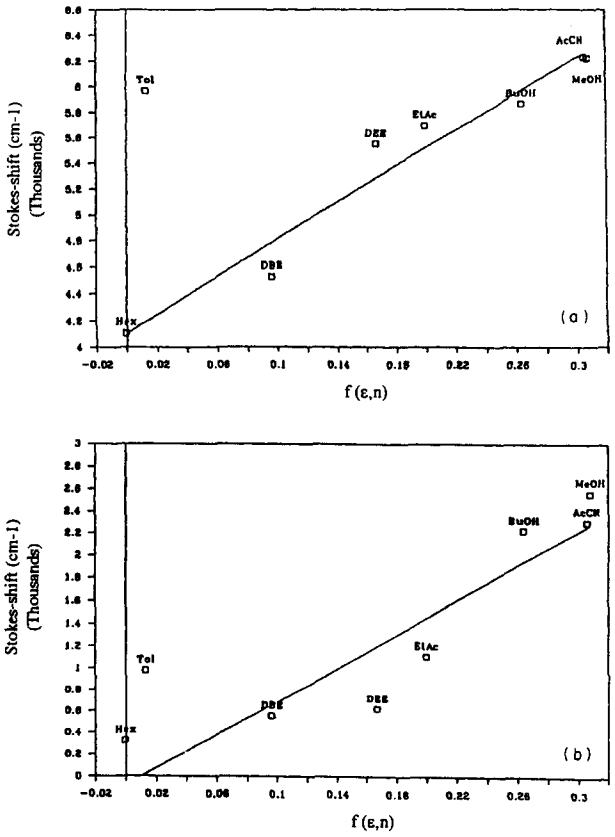

Fig. 8. Solvatochromic plot of the Stokes shift of 9CB (a) and 9CF (b) vs. solvent polarity. $\Delta f(\epsilon,n)$ is the solvent polarity function of Eq. (3). Solvents used are those in Table 3. The least-squares correlation line does not take into account the point for toluene solution.

Table 4
Slopes (m) of the linear regression of Lippert plots (Eq. (3), Stokes shift (cm^{-1}) vs. solvent polarity Δf) for 9CB, 4COB and 9CF and dipole moments of their lowest singlet states for different assumed Onsager radii (a). Upper, part: $a = 0.6$ nm is about 40% of the aromatic system including terminal van der Waals radii. Lower part: different a values representing 40% of the long axis of the molecules including the aliphatic chain

	9CB	4COB	9CF
m (cm^{-1})	7073	12648	7684
a (nm)	0.6	0.6	0.6
$\Delta\mu$ (D)	12.4	16.4	13.0
μ_1* (D)	17.1	21.4	17.7
a (nm)	0.9	0.75	0.9
$\Delta\mu$ (D)	22.9	22.0	23.9
μ_1*	27.6	27.0	28.6
μ_0* (D)	4.7	5.0	4.7

*$\mu_1 = \Delta\mu - \mu_0$; μ_0 obtained from Table 5.

their different dipole moments, their relative order depends on the solvent polarity (the calculations refer to the gas phase).

(2) The difference between S_1 for the planar and perpendicular conformations is approximately 0.1 eV in all cases. To this value, the ground state destabilization energy of 0.1 eV [24] must be added, such that the absolute energetic destabilization of S_1 by twisting from 0° to 90° will be of the order of 0.2 eV only.

(3) Complication arises in the case of DMA-CB where, for the planar conformation, S_1 is of ^1L_a nature, but of ^1L_b nature for 90° twisting. This angle-dependent state crossing has also been observed for terphenyls [9].

(4) The energy gap between the lowest energy conformation of the delocalized excited (DE) S_1 state (S_1, planar) and the lowest energy TICT state conformation (90° twist, S_3 to S_4 in the gas phase, see Table 5) diminishes with increasing donor strength (Table 6), and inclusion of solvent stabilization can bring this TICT state energetically below the DE state including the ground state destabilization (Table 6).

(5) Table 5 also contains the calculated results for the compound cyano-9-anthryl-dimethylaniline (CNADMA), labelled here as DMA-CAP (Fig. 9) to underline its identity as the dibenzo derivative of DMA-CB. This compound shows very strong TICT state formation in solution. The TICT state formation of CNADMA, ADMA and several model compounds has been studied extensively [25–31].

The results in Table 5 indicate that the energy gap between the S_1 and TICT states for the 90° conformation is similar for DMA-CB and DMA-CAP (about 0.7 eV in the gas phase), and therefore both compounds should possess a similar TICT state formation tendency if the DE–TICT energy gap is the only important factor. Yet the experiments indicate a very different behaviour: TICT state formation for DMA-CAP, none for DMA-CB. In addition, for an anilino-pyridinium derivative of similar structure, a strong solvent polarity and viscosity dependence was observed and assigned to TICT state formation in accordance with quantum chemical calculations [32]. Possible explanations for this discrepancy may be that there is an energy barrier between the DE and TICT states for DMA-CB, which is strongly reduced in the case of DMA-CAP, or that the equilibrium twist angle of the DE state is an important factor. It is close to 0° for DMA-CB, but probably around 60° for DMA-CAP. For the related ADMA, it has recently been measured by jet spectroscopy to be 60° for S_1 (DE) and 90° for S_0 in the gas phase [33]. The reason for the larger equilibrium twist angle of the anthracene derivatives is the strong steric hindrance to planarity. This steric destabilization potential present in planar conformations will help to overcome energy barriers which may be present along the TICT state formation pathway, and sterically hindered biphenyl derivatives are thus likely candidates for TICT state behaviour.

Table 5
Results of quantum chemical calculations (CNDO/S) on planar and twisted cyanobiphenyl (CB) model compounds in the gas phase as a function of increasing donor strength (1O, methoxy; A, amino; DMA, dimethylamino)

Compound	Conformation angle (°)	State	E (eV)	f	μ (D)
CB	Planar	S_0			4.7
		S_1 (^1L_b)	4.49	0	8.3
		S_2	4.59	0	4.3
		S_3 (^1L_a)	4.60	0.47	9.9
	90	S_1	4.63	0.0002	4.9
		S_5 (TICT)	5.72	0	25.6
1COB	Planar	S_0			5.0
		S_1 (^1L_b)	4.44	0.0069	8.3
		S_2 (^1L_a)	4.47	0.42	12.2
		S_3	4.48	0.081	6.8
	90	S_1	4.55	0.015	7.5
		S_4 (TICT)	5.42	0	27.7
A-CB	Planar	S_0			5.4
		S_1 (^1L_b)	4.38	0.0090	6.8
		S_2 (^1L_a)	4.40	0.5	15.8
		S_3	4.46	0.0013	9.7
	90	S_1	4.46	0.021	8.9
		S_4 (TICT)	5.28	0	29.8
DMA-CB	Planar	S_0			6.1
		S_1 (^1L_a)	4.34	0.24	12.5
		S_2	4.35	0.31	14.0
		S_3 (^1L_b)	4.35	0.0011	12.2
	90	S_1	4.42	0.023	10.4
		S_3 (TICT)	5.13	0	32.2
DMA-CAP	90	S_1 (^1L_a)	3.15	0.25	5.3
		S_3 (TICT)	3.93	0	28.1

All angles are idealized (trigonal or tetrahedral). Bond length (Å): C–C(aromatic) = 1.4; N–C–ring = 1.158, 1.42; ring–ring = 1.54; ring–O–Me = 1.37, 1.46; ring–N–Me = 1.37, 1.46; all bonds to protons = 1.08. E, state energy with respect to S_0 for a given conformation; f, oscillator strength; μ, dipole moment.

Table 6
Calculated energy gap ΔE(TICT) (eV) between S_1 (planar conformation) and the TICT state as a function of solvent polarity[a]

Compound	ΔE (TICT) (eV)		
	Gas phase	In hexane	In acetonitrile
CB	+1.33	+1.12	+0.77
1COB	+1.08	+0.85	+0.47
A-CB	+1.00	+0.72	+0.27
DMA-CB	+0.89	+0.59	+0.12[b]

[a]Solvent stabilization according to

$$\Delta E(\text{TICT}) = \Delta E_{\text{destab}}\ (S_0, 90°) + \{E(\text{TICT}) + \Delta E_{\text{solv}}(\text{TICT})\} - \{E(S_1) + \Delta E_{\text{solv}}(S_1)\}$$

The ground state destabilization of the 90° twisted conformation (ΔE_{destab}) was taken as 0.1 eV [22]. The solvent stabilization energy $\Delta E^{\text{solv}}(S_n)$ of state n was calculated using [23]

$$\Delta E_{\text{solv}}(S_n) = -\frac{\mu^2(S_n)}{4\pi\epsilon_0 a^3} f(\epsilon),\ f(\epsilon) = \frac{\epsilon - 1}{2\epsilon + 1}$$

An intermediate value of 0.7 nm was assumed for a.

[b]For $a = 0.6$, a value of -0.3 eV is found in acetonitrile.

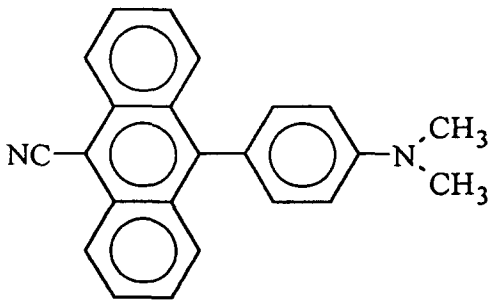

DMA-CAP

Fig. 9. Structure of CNADMA (DMA-CAP).

3.3. Time-resolved excimer fluorescence in neat phases

For the formation of excimers in bulk phases, two monomer units must come close to one another to form a sandwich pair. It has been suggested from X-ray data that these pairs are preformed in the ground state, and that their overlap is such that the length of the dimer becomes about 1.6 times the monomer length [34]. Time-resolved measurements can help to clarify

the question of preformation, because if rearrangement is not necessary for excimer formation from the preformed dimer, no excimer rise times should be observed.

In addition to short, more fully overlapping and more extended, only partially overlapping sandwich-type structures Scheme 1 near here please (Scheme 1, (a) and (b)), another excimer structure can be proposed involving a self-solvated TICT state (Scheme 1, (c)), i.e. a TICT molecule interacting with a ground dipole of the same species [8]. The planar model compound 9CF can help to clarify this. Fig. 10 displays the time-resolved spectra for 9CF and 9CB in the crystalline phase. For these conditions, the weight of excimer fluorescence is comparatively low for 9CB, whereas it increases to about 100% on transition to the mesophase [2]. In planar, bridged 9CF, the weight of the excimer component in the crystalline phase is considerably larger. This can also be seen by the large weight of the long decay times in the longer wavelength region.

By analysing the decay curves taken at many emission wavelengths (spaced at 10 nm intervals) globally, satisfactory fits can be obtained with a three-exponential model. We therefore conclude that three emissive species contribute to the observed fluorescence spectrum.

At short wavelengths, spectrally close to the emission of the 9CF monomer in dilute solution, a decay component of approximately 200 ps is observed. At long wavelengths ($\lambda > 380$ nm), this component is seen as a rise time, together with decay components of 1.8 ns (maximal weight at 380 nm) and 25 ns (maximal weight

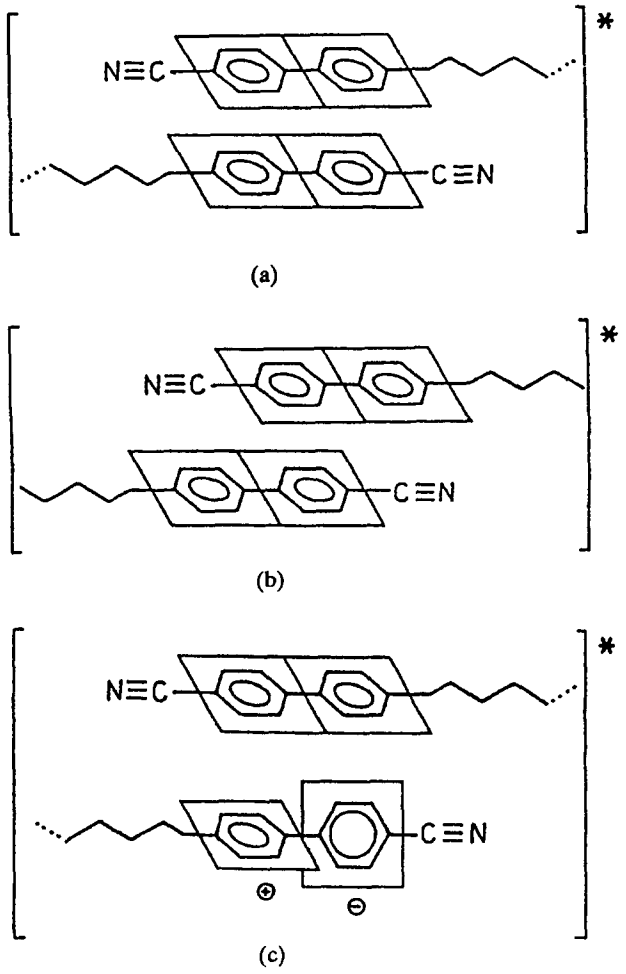

Scheme 1. Different possible *n*C(O)B excimer structures: (a) and (b) shortened and elongated sandwich-type excimers; (c) self-solvated TICT excimer.

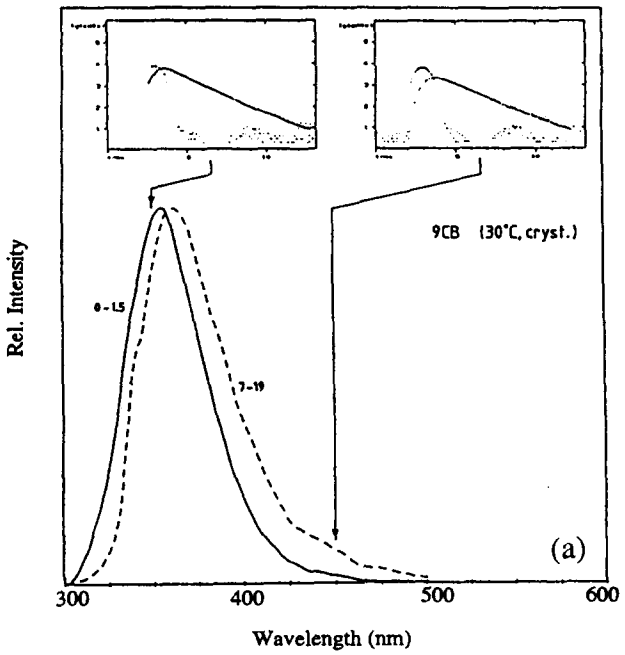

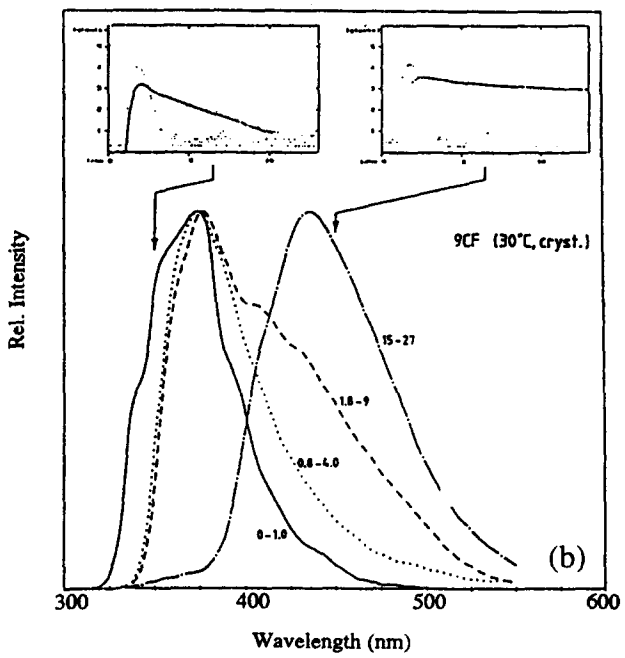

Fig. 10. Normalized time-resolved emission spectra at different time windows for 9CB (a) and 9CF (b) in the crystalline phase (at about 30 °C). The insets show the decay curves at 350 nm and 450 nm; excitation at 250 nm.

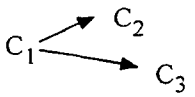

Scheme 2. Simultaneous formation of excimers from a common precursor.

Table 7
Fluorescence decay times (ns) of different alkyl- and alkoxycyanobiphenyls and the model compound 9CF in neat phases (temperature dependent) at 350 nm (excitation at about 260 nm). Relative emission yields Y_{rel}[c] for the short-lived component τ_1 are also given

Compound	Phase (T) (°C)	τ_1[a]	Y_{rel}[a] (%)	τ_2	τ_3
9CB	C (33)			1.24	
	S_A (44)	0.14	6		14.4
	N (49)	0.12	7		11.9
	I (69)	0.04	4		8.0
9COB	C (45)			1.0	13.0
	S_A) (70)	0.06	3		11.6
	N (79)	0.06	3		8.5
	I (86)	0.06	5		5.7
9CF	C (36)	0.23	32	1.66	[b]
	I (76)	0.24	6		14.5

[a]The τ_1 values (less than 0.1 ns) are uncertain, because they are beyond the resolution of our equipment. However, the relative emission yield (Y_{rel}) of this component, is relatively stable.

[b]About 20 ns can be resolved starting from about 390 nm (Y_{rel} of this component at 450 nm is about 80%).

$$^{c}H_{rel} = \frac{\alpha_i \tau_i}{\sum_i \alpha_i \tau_i}$$

at around 420 nm) (compare the insets in the time-resolved spectra, Fig. 10(b)). This behaviour could be consistent with one precursor (monomer) feeding two products (excimers) with different decay times (Scheme 2).

Above the melting point, only one product component is observed probably due to a fast equilibrium in either the ground or excited state. This is shown in Table 7 which also contains the corresponding data for 9CB.

4. Conclusions

By analysis of the temperature dependence of the fluorescence band shapes of 9CB and 4COB and comparison of the fluorescence rise times, we have shown that the phenyl rings of cyanobiphenyl compounds relax towards planarity in the excited state. This was confirmed by investigating a bridged model compound (9CF) with an enforced planar conformation. The similar solvatochromic behaviour of 9CB and 9CF does not support the formation of a TICT state in dilute solution, although quantum chemical calculations indicate that this state may be within energetic reach in polar solvents. Comparable luminescence behaviour for unbridged and bridged compounds was also found for neat phases. In the crystalline phase, bridged 9CF forms excimers more efficiently than 9CB. In liquid crystalline phases and/or in the isotropic melt, all nC(O)B compounds form long-lived, excimer-like aggregates within about 100 ps. Taken together, these data support a model of planar preformed pairs of chromophores in the cyanobiphenyl liquid crystals.

Acknowledgements

We wish to thank Michael Schulz, Free University Berlin, for the gift of purified 9CF and Dr. R. Lapouyade for the gift of DMA-CB. We also wish to thank the group of Professor G. Heppke, Berlin, for providing us with some of the commercially available samples. Financial support by the Bundesministerium für Forschung und Technologie (Project 05314 FAI5) and the Deutsche Forschungsgemeinschaft is also gratefully acknowledged.

Financial support in the form of a scholarship from K.U. Leuven to J. Hofkens and from ICI to M. van Damme is gratefully acknowledged, as well as the continuous support to our laboratory by the Belgium National Science Foundation and the Ministry of Science Programming through IUAP-II-1 and IUAP-III-040. Professor N. Boens is thanked for the development of the software used in the fluorescence decay analysis.

References

[1] D. Baeyens-Volant and C. David, *Mol. Cryst. Liq. Cryst., 116* (1985) 217.
[2] D. Markovitsi and J.P. Ide, *J. Chim. Phys., 83* (1986) 97.
[3] N. Tamai, I. Yamazaki, H. Masuhara and N. Mataga, *Chem. Phys. Lett., 104* (1984) 485.
[4] R. Subramanian, L.K. Patterson and H. Levanon, *Chem. Phys. Lett., 93* (1982) 578.
[5] M. van Damme, J. Hofkens, F.C. De Schryver, T.G. Ryan, W. Rettig and A.M. Klock, *Tetrahedron, 45* (1989) 4693.
[6] C. David and D. Baeyens-Volant, *Mol. Cryst. Liq. Cryst., 59* (1980) 181.
[7] (a) Z.R. Grabowski, K. Rotkiewicz, K. Retakes, A. Siemiarczuk, D.J. Cowley and W. Baumann, *Nouv. J. Chim., 3* (1979) 443; (b) W. Rettig, *Angew. Chem., 98* (1986) 969; *Angew. Chem. Int. Ed. Engl., 25* (1986) 971; (c) U. Leinhos, W. Kühnle and K.A. Zachariasse, *J. Phys. Chem., 95* (1991) 2013.
[8] Z.R. Grabowski, K. Rotkiewicz, H. Leismann and W. Rettig, *J. Photochem. Photobiol. A: Chem., 49* (1989) 347.
[9] G. Swiatkowski, R. Menzel and W. Rapp, *J. Lumin., 37* (1987) 183.
[10] M. Van den Zegel, N. Boens, D. Deams and F.C. De Schryver, *Chem. Phys., 111* (1984) 340.
[11] D.W. Marquardt, *J. Soc. Ind. Appl. Math., 2* (1963) 431.

[12] (a) L.D. Janssens, N. Boens, M. Ameloot and F.C. De Schryver, *J. Chem. Phys., 94* (1990) 3564–3576; (b) N. Boens, L.D. Janssens and F.C. De Schryver, *Biophys. Chem., 33* (1989) 77–90; (c) J.M. Beechem, M. Ameloot and L. Brand, *Chem. Phys. Lett., 120* (1985) 466–472.

[13] (a) W. Rettig, M. Vogel and A.M. Klock, *EPA Newsl., 26* (1986) 41; (b) M. Vogel and W. Rettig, *Ber. Bunsenges. Phys. Chem., 91* (1987) 1241.

[14] J. Del Bene and H.H. Jaffé, *J. Chem. Phys., 48* (1986) 1807, 4050; *49* (1986) 1221; *50* (1969) 1126.

[15] Updated version of program CNDUV99, *QCPE 333*, Quantum Chemistry Program Exchange, Bloomington, IN.

[16] (a) N. Mataga, H. Jao, T. Okada and W. Rettig, *J. Phys. Chem., 93* (1989) 3383; (b) W. Rettig, *Ber. Bunsenges. Phys. Chem., 95* (1991) 259; (c) H. Sumi and R.A. Marcus, *J. Chem. Phys., 84* (1986) 4894.

[17] (a) G.K. Schenter and C.B. Duke, *Chem. Phys. Lett., 176* (1991) 563; (b) G.J. Moro, P.L. Nordio and A. Polimeno, *Mol. Phys., 68* (1989) 1131; (c) G. Giacometti, G.J. Moro, P.L. Nordio and A. Polimeno, *J. Mol. Liq., 42* (1989) 19.

[18] E. Lippert, *Z. Naturforsch., Teil A, 10* (1955) 541.

[19] E. Lippert, *Ber. Bunsenges. Phys. Chem. (Z. Elektrochem.), 61* (1957) 962.

[20] A.M. Klock and W. Rettig, unpublished results, 1992.

[21] A.M. Klock and W. Rettig, *Pol. J. Chem., 67* (1993) 1375.

[22] F. Momicchioli, I. Baraldi and M.C. Bruni, *J. Chem. Phys., 70* (1982) 161.

[23] C.J.F. Böttcher, *Theory of Electric Polarisation*, Vol. 1, Elsevier, Amsterdam, 1973, p. 145.

[24] A. Almeningen, O. Bastiansen and L. Fernholt, *J. Mol. Struct., 128* (1985) 59.

[25] W. Baumann, B. Schwager, N. Detzer, T. Okada and N. Mataga, *J. Phys. Chem., 92* (1988) 3742.

[26] T. Okada, T. Fujita, M. Kubota, S. Masaki, N. Mataga, R. Ide, Y. Sakata and S. Misumi, *Chem. Phys. Lett., 14* (1972) 563.

[27] A. Siemiarczuk, Z.R. Grabowski, A. Krówczynski, M. Asher and M. Ottolenghi, *Chem. Phys. Lett., 51* (1977) 315.

[28] W. Baumann, F. Petzke and K.-D. Loosen, *Z. Naturforsch., Teil A, 37* (1982) 598.

[29] A. Siemiarczuk, *Chem. Phys. Lett., 110* (1984) 437.

[30] N. Detzer, W. Baumann, B. Schwager, J.-C. Fröhling and C. Brittinger, *Z. Naturforsch., Teil A, 42* (1987) 395.

[31] T. Okada, N. Mataga, W. Baumann and A. Siemiarczuk, *J. Phys. Chem., 91* (1987) 4490.

[32] H. Ephardt and P. Fromherz, *J. Phys. Chem., 95* (1991) 6792.

[33] O. Kajimoto, S. Hayami and H. Shizuka, *Chem. Phys. Lett., 177* (1991) 219.

[34] (a) P.E. Cladis, D. Guillon, E.R. Bouchet and P.L. Finn, *Phys. Rev. A, 23* (1981) 2594; (b) L. Longa and W.H. de Jeu, *Phys. Rev. A, 26* (1982) 1632; (c) D. Guillon and A. Skoulios, *J. Phys., 45* (1984) 607.